Adiabatic Film Cooling Effectiveness From Heat Transfer Measurements in Compressible, Variable-Property Flow

P. M. Ligrani[1]
C. Camci
Von Karman Institute for Fluid Dynamics,
Chaussee de Waterloo, 72
B-1640 Rhode-St.-
Genese, Belgium

A variable property correction is given for turbulent boundary layers that are film-cooled using staggered rows of injection holes inclined at 35 deg. With the correction, a relation is provided between the adiabatic film cooling effectiveness for constant property flow and heat transfer coefficients for variable property flow, which are based on the difference between the freestream recovery temperature and wall temperature. The variable property correction was determined from heat transfer measurements for a range of injection parameters at different values of the nondimensional coolant temperature and from results in the literature. Because the flow is compressible, the importance of the injection mass flux ratio, momentum flux ratio, and velocity ratio are considered in the determination of effectiveness.

1 Introduction

Designers of film-cooled components require a detailed knowledge of convective heat transfer processes which occur when a coolant is injected into a boundary layer. Such knowledge is required since film cooling allows a means to protect gas turbine parts, such as turbine blades and combustion chamber linings, from the thermal loading that results from exposure to hot gases. Much information on these processes is available from fundamental studies employing laboratory models having a variety of film cooling injection configurations. Consequently, the relationship between heat transfer in the laboratory studies and that in application require understanding, particularly when constant property results are used to design components exposed to variable-property compressible flows.

In comparison to the large temperature differences that exist between the gas and the surface of turbine blades, the blade surface temperature distribution is relatively isothermal. Thus, in regard to thermal boundary layers developing over a turbine blade surface, a blade designer would naturally be more concerned with data obtained using isothermal wall boundary conditions, rather than data obtained when the wall is exposed to a uniform heat flux. However, adiabatic wall boundary conditions are a subset of the latter type of thermal boundary condition and are advantageous in that they may be used to describe the convection processes that occur during film cooling in an economical way. Such economy is provided because a problem having three temperature potentials, T_∞, T_c, and T_W, is reduced to a two temperature one. In this case, the heat flux in incompressible flow with film cooling is given by

$$\dot{q}''_w = h_f (T_{AW} - T_W) \tag{1}$$

where T_{AW} may be expressed nondimensionally using adiabatic film cooling effectiveness, η. The magnitudes of h_f and T_{AW} are generally determined from spanwise averages of local measurements of these two quantities [1-5]. Other investigations [6-7] describe convective film-cooling processes using isothermal wall boundary conditions along with the equation

$$\dot{q}''_w = h (T_{o\infty} - T_w) \tag{2}$$

Here, h is provided with the temperature of the injected fluid, often expressed nondimensionally using θ.

The connection between the two approaches given by equations (1) and (2) began with a study by Metzger et al. [8], who showed the linear dependence of h/h_o on θ for a variety of injection conditions in constant property flow. In a discussion of this paper, E.R.G. Eckert pointed out that the horizontal and vertical intercepts of such plots gave $1/\eta$ and h_f/h_o, respectively. From these two sources, equations (1) and (2) are set equal, and definitions for η and θ are used to give

$$h = h_f (1 - \eta\theta) \tag{3}$$

Dividing by h_o then produces

$$\frac{h}{h_o} = \frac{h_f}{h_o} (1 - \eta\theta) \tag{4}$$

In an investigation involving both slot and discrete hole injection, Metzger and Fletcher [9] then used this approach to obtain η. Eckert et al. [10] compared η determined from these measurements to results from the University of Minnesota and found differences ranging from 0 to 20 percent over a range of conditions. These differences for injection from a single row of holes may have resulted since Metzger and Fletcher's [9] measurements provide a global adiabatic film-cooling effectiveness, instead of a spatial average of effectiveness determined from measurements on a surface which is locally adiabatic. In a more recent paper, Eckert [11] provides additional discussion of the connection between equations (1) and (2). Here, he shows how results from one method can be transformed into parameters used in the other as applied to full-coverage film cooling. Several studies [3-5, 12] have also focused on the effects of density ratio ρ_c/ρ_∞, compressibility, and/or large temperature differences on film-cooled boundary layers; however, none of these have addressed the connection between adiabatic and isothermal boundary conditions when the effects of variable properties are important.

Consideration of the connection between heat transfer measured with isothermal and adiabatic boundary conditions in film-cooled boundary layers with variable properties requires examination of a number of important factors.

1 The h/h_o versus θ extrapolation procedure used in [8, 9,

[1]Present address: Department of Mechanical Engineering, Naval Postgraduate School, Monterey, Calif. 93943

Contributed by the Heat Transfer Division for publication in the JOURNAL OF HEAT TRANSFER. Manuscript received by the Heat Transfer Division June 6, 1983.

10] is not valid because the energy equation is nonlinear and coupled to the momentum equation. In the present study, a new extrapolation procedure is given for a compressible flow with $M_\infty = 0.64$. In order to account for viscous dissipation, all gas total temperatures in equations (1–4) are replaced by recovery temperatures.

2 The ratio ρ_c/ρ_∞ will change as h/h_o varies with θ in compressible flow. This leads to the question: Which coolant injection parameter, m, I, or U_c/U_∞, should be held constant along a collection of h/h_o versus θ points? Each of these injection parameters is considered in the present extrapolation procedures, and adiabatic film cooling effectiveness is given for constant m, I, and U_c/U_∞.

3 Determination of η from isothermal wall heat transfer measurements requires that

$$\overline{h_i'\ (T_{AW}' - T_W)} = \overline{h_f'(T_{AW}' - T_W)} \tag{5}$$

which is true at a given downstream location only when local h_f' and η' are invariant in the spanwise direction and equal to spanwise averaged values, h_f and η. In the design of the present experiment, two staggered rows of injection holes were chosen instead of say, one row, to give a spanwise uniform flow for $x/d > 20$. Inequality of equation (5) is discussed for results obtained when $x/d < 20$.

With these three points in mind, the primary objective of the present study is to povide a connection between heat transfer in film-cooled boundary layers with variable properties and isothermal wall boundary conditions, and those with constant properties and adiabatic boundary conditions. Empirical variable property correction terms are introduced into equation (4) for this purpose. Thus experimental results are given leading to a relationship between the two types of measurements that are generally made in film-cooled boundary layers: (*i*) η and h_f, and (*ii*) h at specific values of θ, where the former are for a constant property environment, and the latter are for a variable property environment. The variable property results consist of heat transfer coefficients based on the $(T_{r\infty} - T_w)$ temperature difference which were measured at similar M_∞, Reynolds numbers, and $T_{rc}:T_{r\infty}:T_w$ ratios as exist in the flow near gas turbine blades. The constant property η and h_f were measured by Jabbari and Goldstein [1] and Jabbari [2]. The present model was designed to be geometrically similar to theirs, including the test surface boundary layer and injection geometry.

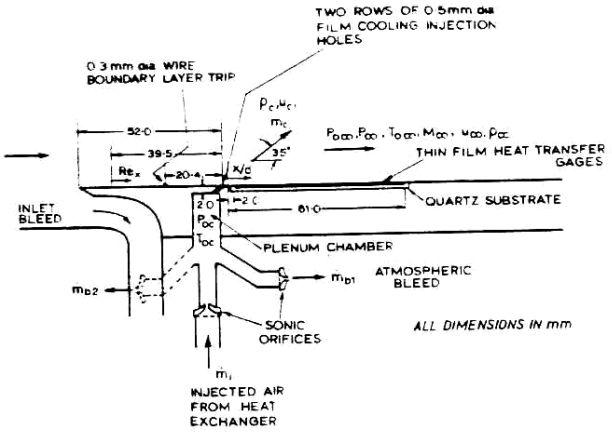

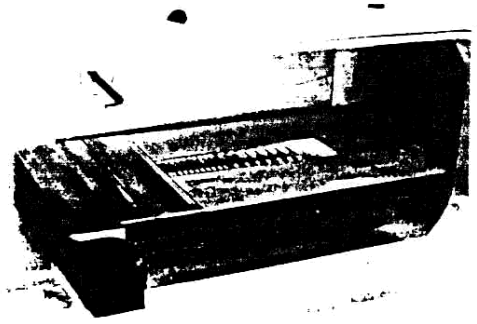

Fig. 1 Test model

2 Experimental Facility and Measurement Techniques

(*a*) Model and Test Facility. The model used for testing is shown in Fig. 1. The photograph shows installation in the CT-2 compression tube facility described by Ligrani et al. [13], Consigny et al. [14] and similar in operation to a facility

Nomenclature

A = injection hole area
C_D = discharge coefficient
C_p = specific heat at constant pressure
d = injection hole diameter
h, h_f = heat transfer coefficients with film cooling (spanwise averaged), $\dot{q}_w''/(T_{r\infty} - T_w)$, $\dot{q}_w''/(T_{AW} - T_w)$
h_o = heat transfer coefficients without film cooling (spanwise averaged), $\dot{q}_{wo}''/(T_{r\infty} - T_w)$
I = injection momentum flux ratio, $\rho_c U_c^2/\rho_\infty U_\infty^2$
l = length of injection holes
m = injection mass flux ratio, $\rho_c U_c/\rho_\infty U_\infty$
$\dot{m}_c$ = injection mass flow rate, equation (6)
n, p = empirical constants in equation (12)
P = static pressure
Pr = molecular Prandtl number
$\dot{q}_w''$ = wall heat flux with film cooling
$\dot{q}_{wo}''$ = wall heat flux without film cooling
R = gas constant
Re_d = freestream Reynolds number based on diameter of injection holes, $dU_\infty\rho/\mu$
Re_x = freestream Reynolds number based on downstream distance measured from effective origin of turbulent boundary layer
St = Stanton number, $h_o/\rho_\infty U_\infty C_p$
T = static temperature
U = mean velocity
x = distance from downstream edge of injection holes
δ_1 = boundary layer displacement thickness at upstream edge of injection holes
ρ = density
η = adiabatic film cooling effectiveness (spanwise averaged), $(T_{AW} - T_{r\infty})/(T_{rc} - T_{r\infty})$
μ = absolute viscosity
θ = nondimensional coolant temperature, $(T_{rc} - T_{r\infty})/(T_w - T_{r\infty})$

Subscripts

AW = adiabatic wall
c = coolant
i = isentropic
o = total condition
r = recovery condition
W = wall
∞ = freestream

Superscripts

$'$ = local value
$-$ = spanwise average
$\hat{}$ = variable property

described in [15]. CT-2 provides a high-pressure, high-temperature environment for testing by means of an isentropic compression of air by a lightweight piston driven by a high-pressure air supply. When the air in front of the piston reaches the desired pressure level, a fast opening shutter valve is activated allowing flow into the test section. Steady conditions may then be produced for periods as long as several seconds, during which time the same Reynolds numbers, Mach numbers, and $T_{r\infty}:T_{rc}:T_w$ ratios may be produced as exist in the first turbine stage of a gas turbine engine.

For the present tests, the total pressure and temperature in the model free stream were approximately 2.9×10^5 N/m^2 absolute, and 403 K, respectively. The magnitude of T_w was about 290 K. Visualization using a row of surface oil drops showed the flow over the test model to be spanwise uniform. The free-stream Mach number was 0.64 and maintained at this value during test durations using a sonic throat downstream of the test section. The zero pressure gradient was adjusted by means of a valve for the inlet bleed slot, shown in Fig. 1, and measured using a row of static pressure tapings extending from the plate leading edge to the end of the instrumented surface. A zero pressure gradient along the entire length of the test plate also ensured that streamlines approaching the leading edge were parallel to the plate surface.

The model used was geometrically similar to the one described by Jabbari and Goldstein [1] and Jabbari [2]. The magnitude of δ_1/d in the present study was approximately 0.16, compared to 0.177 for Jabbari's work. This magnitude of δ_1/d was obtained by placing a 0.3-mm-dia wire trip 20.4 mm upstream of the rows of film-cooling holes, as shown in Fig. 1. The trip was located in order to assure laminar-turbulent transition, as well as to provide the appropriate boundary layer thickness according to correlations presented by Schlichting [16]. From the turbulent boundary layer correlation for boundary layer displacement thickness, the effective origin of the layer was also determined in order to provide the location for measurement of Re_x.

The 0.5-mm-dia injection holes were inclinded at an angle of 35 deg and spaced 3 dia apart in the spanwise direction. A total of 101 injection holes were contained in two rows spaced 2.5 dia apart. The holes in the rows were staggered with respect to each other so that the midspan distance between two holes in the same row located the center line of holes in the adjacent row. For all runs in the present test program, the Reynolds numbers were high enough to ensure that the injectant was turbulent. The magnitude of the mainstream Reynolds number based on hole diameter Re_d in the present study was 1.1×10^4 compared to 10^4 and 2.1×10^4 for [1]. The temperature of the injected air was varied by means of a regenerative heat exchanger, which provided air for the injectant plenum chamber at rates measured using a sonic orifice. Two atmospheric bleed sonic orifice passages were also connected to the plenum chamber in order to reduce the time required to inject film cooling air over the test surface, and to minimize transient effects in the plenum chamber that may occur at shutter opening when freestream air abruptly moves into the test section. The uniformity of the plenum chamber pressure P_{oc} was found to be satisfactory over a range of injection conditions, after measurement at three different spanwise locations.

Pressures were measured using National Semiconductor and Validyne variable reluctance pressure transducers, connected as near as possible to measurement locations to minimize response time. Temperatures were measured using thermocouples consisting of 0.05-mm-dia chromel-alumel wire with welded junctions. Each pressure and temperature sensor was calibrated individually with respect to a known reference for the range of measurement conditions. Recovery temperatures were calculated using a recovery factor equal to $Pr^{1/3}$ (Kays and Crawford [17]).

Referring to Fig. 1, the mass flow rate of the coolant was calculated using

$$\dot{m}_c = \dot{m}_t - \dot{m}_{b1} - \dot{m}_{b2} \tag{6}$$

Knowing the injection area A, the injection mass flux rate then followed from the equation

$$\rho_c U_c = \dot{m}_c / A \tag{7}$$

As injectant properties were desired at the exit of the injection holes, coolant static density and total temperature were given by

$$\rho_c = P_\infty / RT_c \tag{8}$$

and

$$T_{oc} = T_c + U_c^2/2C_p \tag{9}$$

respectively. Values of T_{oc}, estimated at the exits of the injection holes, were used in equation (9). These values of T_{oc} were based on measured plenum chamber coolant temperatures corrected to account for heat transfer from the coolant to the $l/d = 7$ injection hole surfaces. Injection was started 400–700 ms before the mainstream as experience with the facility showed that less significant injection plenum chamber transients exist than if free stream and injection are started at the same time.

Solution of equations (7–9) thus allowed determination of injectant parameters U_c, ρ_c, and T_c, since all other quantities in these equations were measured or estimated from measurements. From isentropic flow relations, the discharge coefficient could then be calculated using

$$C_d = \rho_c U_c / (\rho_c U_c)_i \tag{10}$$

where

$$(\rho_c U_c)_i = P_\infty \left(\frac{P_{oc}}{P_\infty}\right)^{2/7} \left[\frac{7}{RT_{oc}}\left(1 - \left(\frac{P_{oc}}{P_\infty}\right)^{-2/7}\right)\right]^{1/2} \tag{11}$$

With this procedure, m, I, U_c/U_∞, ρ_c/ρ_∞, and C_D were obtained for each test run.

(b) Heat Transfer Measurement. The wall heat flux was measured using thin-film platinum gauges, which may be seen in the photograph of Fig. 1. The gauges had a 1 mm dimension in the x-direction and all x/d values were measured to the gauge centerline. The thin films had a spanwise dimension of 12 mm in order to obtain $\dot{q}_w''$ values averaged across the span. The gauges functioned as resistance thermometers. They were connected to operational amplifiers, which maintained constant current across gauges with respect to time. The voltage outputs from these circuits then passed to electrical circuits with resistances and capacitances arranged to produce voltages and currents proportional to temperatures and heat fluxes. These analogue circuits were constructed to simulate one-dimensional heat transfer into a semi-infinite solid, which required mounting of the thin film gauges on low conductivity quartz substrates. Test model parts were designed and constructed to ensure that conduction in metal parts during tests did not affect the temperature in the quartz or the surface thermal boundary condition.

Because of the abrupt flow of hot gas over the test surface at the beginning of the test, the heat flux variation with time has a steplike behavior. Thin film gauge signal traces showed this step, and also indicated fully turbulent flow over the model test surface. Using the $\dot{q}_w''$ versus time traces, the variation of gauge temperature with time may be constructed mathematically using an inverse transformation [18, 19]. The final result for each gauge was a plot of $\dot{q}_w''$ versus surface temperature which may be then be extrapolated to initial condition, at which time the model surface temperature was uniform. Using this procedure, distributions of $\dot{q}_w''$ were obtained equivalent to those on an isothermal surface.

A thorough discussion of thin film gauge construction and

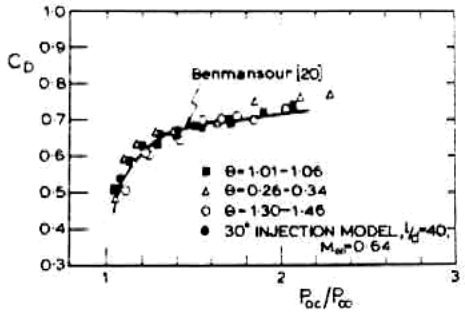

Fig. 2 Film-cooling injection system discharge coefficients

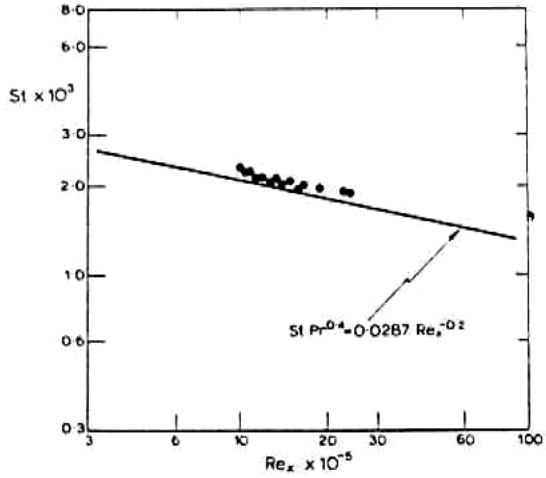

Fig. 3 Baseline heat transfer measurements

measurement details, as applied in the present study, is given in [18].

From the analogue circuits, the signals were sent to amplifier/anti-aliasing filter units which also contained sample and hold devices. The signals were then processed by a multiplexer and analogue-to-digital converter controlled during testing times by a PDP 11/34 computer. The maximum data sampling rate of the system was 500 kHz for the 48 channels, and the signal resolution of the analogue-digital converter was 12 bits. In the present study, a data acquisition rate of 1 kHz, and a sampling time of 512 msec were employed for each channel. In addition to the heat transfer measurements, the system was also used to acquire the output from pressure transducers and thermocouples used to measure various injection and free-stream flow properties during a test run.

3 Baseline Experimental Results

(a) **Discharge Coefficients.** The variation of C_D with P_{oc}/P_{∞} is shown in Fig. 2. The results indicate satisfactory injection system performance since discharge coefficient values do not show a dependence on nondimensional coolant temperature θ. The measured C_D also agree with results from a model having 30-deg injection holes, $l/d = 40$ and $M_{\infty} = 0.64$. C_D values are additionally consistent with results at $M_{\infty} = 0.64$ determined from measurements by Benmansour [20] who employed an injection model having holes inclined at 30 deg with $l/d = 6$.

(b) **Heat Transfer.** Using the procedures described and those given in [18], the baseline results represented in Fig. 3 for zero injection are obtained. The measurements presented in this figure were repeatable within ±3 percent and obtained using the same free-stream conditions described earlier. The data lie just above the flat-plate equation suggested by Kays et al. [17] with maximum differences of about 10 percent. Considering the ±12 percent experimental uncertainty of St (based on a 20:1 confidence level), the results in Fig. 3 provide qualification of heat transfer measurement procedures. These results are also important because they indicate normal boundary layer behavior since the heat transfer is the same as in a normally developing, two-dimensional layer with variable properties. The equation in Fig. 3 is corrected for variable properties using the temperature ratio method of [17]. According to this method, the variable property Stanton number equation is the same as for a constant property environment when $T_w/T_{\infty} < 1$.

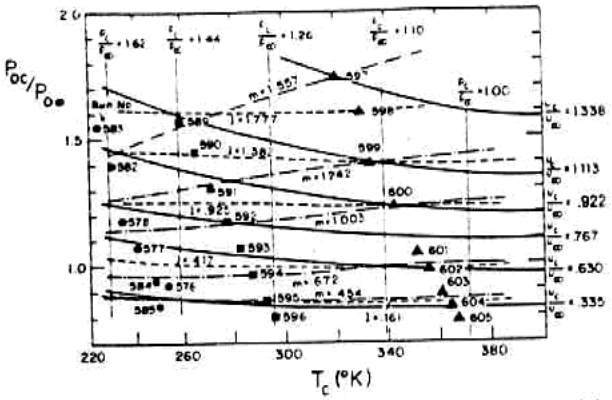

Fig. 4 Experimental operating domain map showing range of injection conditions, • θ = 1.30–1.46, ■ θ = 1.01–1.06, ▲ θ = 0.26–0.34

4 Experimental Results

(a) **Experimental Domain Map.** An experimental operating domain map indicating the range of injection conditions used in the present study is shown in Fig. 4. In the $P_{oc}/P_{o\infty}$ versus T_c coordinates, three sets of data are shown corresponding to cold (θ = 1.30–1.46), ambient (θ = 1.01–1.06) and hot (θ = .26–.34) injection. Lines of constant m, I, U_c/U_{∞}, and ρ_c/ρ_{∞}, determined from measurements at the various data points, show the range of these parameters covered by the present tests. Such results indicate which data runs are required for interpolation in order to obtain information at a constant m, I, or U_c/U_{∞} as the injectant temperature varies. Referring to run number 600, the magnitudes of these three parameters are 1.0, 0.925, and 0.922, respectively. As T_c decreases, the three lines corresponding to these parameter values diverge. Hence, paths followed by injection parameter lines on the domain map differ depending on which injection parameter is held constant. Different injection parameters correspond with different sets of data in variable property flow even though lines representing the injection parameters may intersect at one location on the experimental domain map.

(b) **Heat Transfer Coefficients Based on the $(T_{r_{\infty}} - T_w)$ Temperature Difference.** In Figs. 5–7, heat transfer coefficients with film cooling, $\bar{h}$ are presented for a wide range of experimental conditions. These $\bar{h}$ values are normalized with respect to heat transfer coefficients without film cooling $\bar{h}_{o}$, and plotted versus m, I, and U_c/U_{∞}. The variation of $\bar{h}/\bar{h}_o$ is presented as it varies linearly with m. Magnitudes of I and U_c/U_{∞} were determined from injection calculations for individual runs. Run numbers correspond to those presented in Fig. 4. The data in Figs. 5–7 are plotted parametrically with x/d, showing the variation of $\bar{h}/\bar{h}_o$ with injection parameters at a given downstream location. These plots allow interpolation along $\bar{h}/\bar{h}_o$ curves at values of m, I or U_c/U_{∞} between those at measurement points.

The results in Figs. 5, 6, and 7 are presented for θ values of

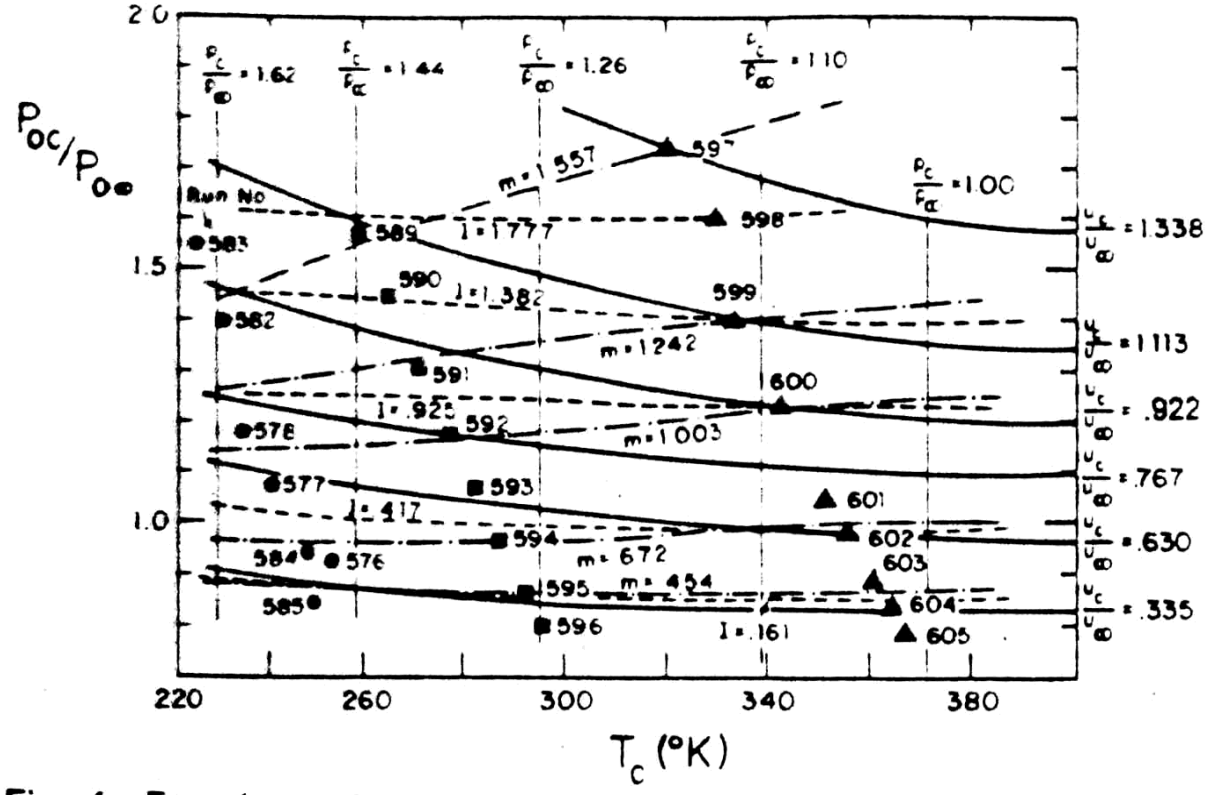

Fig. 4 Experimental operating domain map showing range of injection conditions, ● θ = 1.30–1.46, ■ θ = 1.01–1.06, ▲ θ = 0.26–0.34

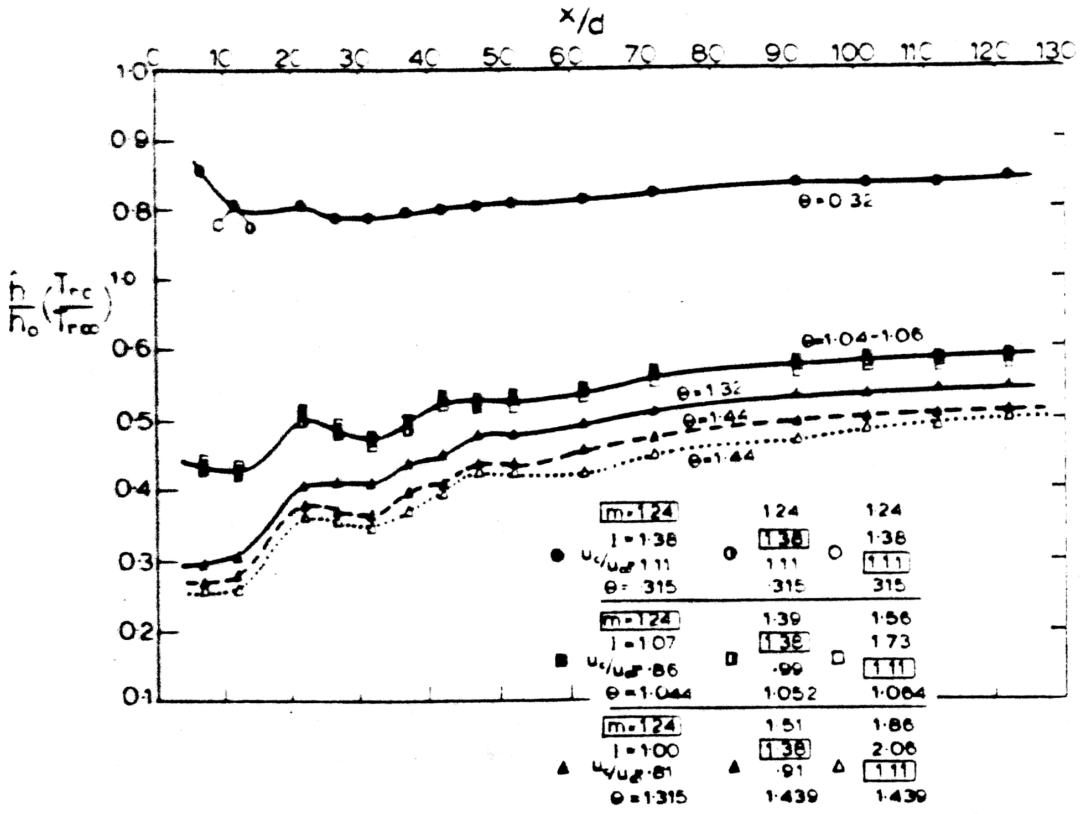

Fig. 9 Variation of $h/h_o(T_{rc}/T_{r\infty})^{1.0}$ with x/d

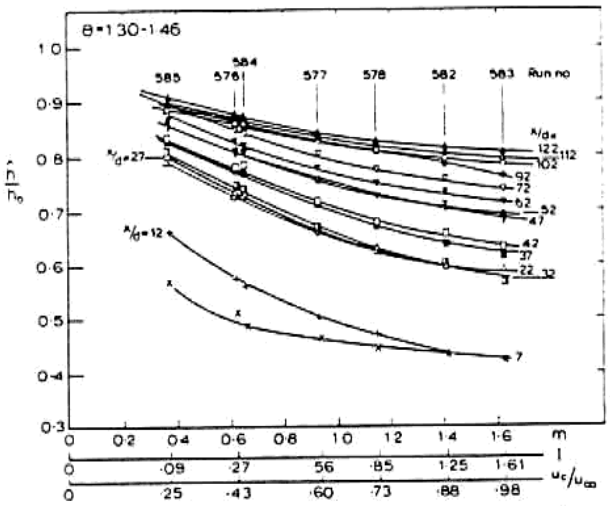

Fig. 5 Normalized heat transfer coefficients with film cooling at different x/d as a function of varying injection parameters

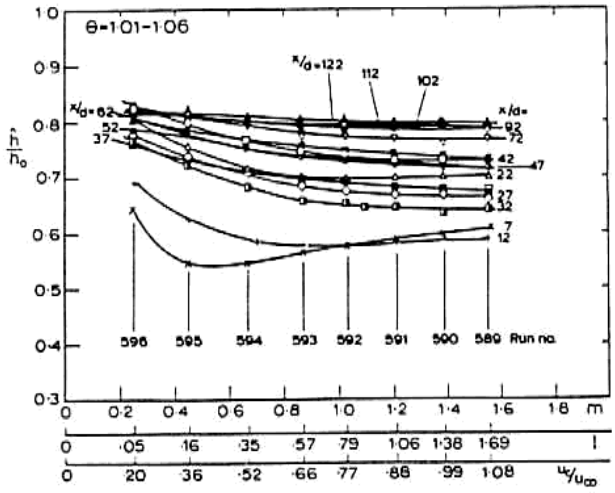

Fig. 6 Normalized heat transfer coefficients with film cooling at different x/d as a function of varying injection parameters

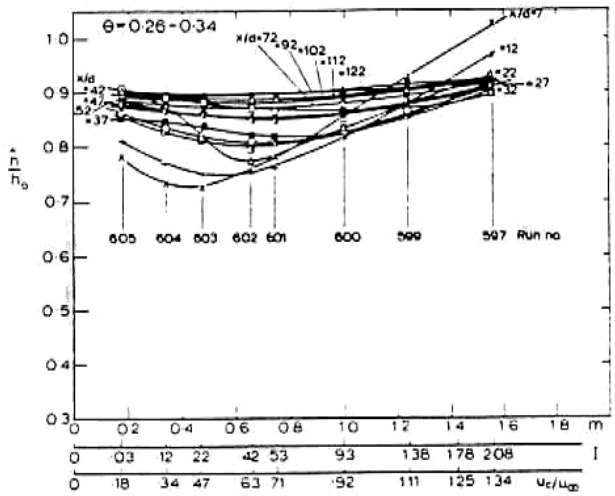

Fig. 7 Normalized heat transfer coefficients with film cooling at different x/d as a function of varying injection parameters

x/d	7	12	22	27	32	37	42	47	52	62	72	92	102	112	122
symbol	×	+	△	◇	◨	■	□	▽	◑	▼	▽	●	○	△	▲

1.30–1.46, 1.01–1.06, and 0.26–0.34, respectively. From these three figures, the largest variations of $h/\bar{h}_o$ with m occur near the injection location at small x/d. At larger x/d locations, farther downstream, the variation of $h/\bar{h}_o$ with m is smaller. Generally, at a given value of m, $h/\bar{h}_o$ increases as x/d increases, where the largest variations occur when θ = 1.30–1.46. Exceptions are evident at high injection rates when θ = 1.01–1.06.

In Fig. 5, minimum values of $h/\bar{h}_o$ occur for magnitudes of m greater than 1.4. In the two following figures, the m where $h/\bar{h}_o$ curves are minimum have smaller magnitudes. In Fig. 7, the $h/\bar{h}_o$ versus m curves pass through well defined minimum regions only when $x/d < 22$. The magnitudes of the normalized heat transfer coefficients in this figure are also closer to 1.0 than measurements at θ = 1.0–1.06 and θ = 1.30–1.46.

(c) Variable Property Correction. In order to account for variable properties in equation (4), the left-hand side is multiplied by $(T_{rc}/T_{r\infty})^n (T_{r\infty}/T_w)^p$ to give

$$h/\bar{h}_o (T_{rc}/T_{r\infty})^n (T_{r\infty}/T_w)^p = h_f/h_o(1-\eta\theta) \tag{12}$$

The $(T_{rc}/T_{r\infty})^n (T_{r\infty}/T_w)^p$ term is then an empirical correction for the influence of temperature-dependent fluid properties in film-cooled turbulent boundary layers. With the correction, a relation is provided between constant property h_f/h_o, constant property adiabatic film cooling effectiveness, and variable property $h/\bar{h}_o$.

Results which follow show that $(T_{rc}/T_{r\infty})^n$ is included in equation (12) so that adiabatic effectiveness results from the presnt study match those from the University of Minnesota [1, 2]. Determination of η is independent of $(T_{r\infty}/T_w)^p$ in equation (12) since $T_{r\infty}$ and T_w are constant regardless of the value of θ. For $m > .65$, empirical constant n is set equal to 1.00, and for $m = .48$, n is set equal to 0.80 in order to obtain: (*i*) data points along straight lines in $h/\bar{h}_o (T_{rc}/T_{r\infty})^n$ versus θ coordinates, and (*ii*) the best fit to η measurements from constant property flows. n is thus dependent on the blowing ratio m.

The variable property correction is consistent with results given by Pedersen, Eckert, and Goldstein [3] and Papell and Trout [21], because equation (12) gives $h/\bar{h}_o$, which are dependent on $T_{rc}/T_{r\infty}$. According to [3], in constant property situations, the adiabatic film cooling effectiveness is a function of a number of parameters, including the injection geometry, the turbulence, the Reynolds number in the mainstream, and the mass flux ratio m. The authors go on to say that "for variable property flows involving ideal gases with transport properties which can be expressed by a power law, the heat transfer and the film effectivenesses are, in addition, a function of the ratio of the absolute temperatures T_∞/T_c or of the density ratio ρ_∞/ρ_c."

The $(T_{r\infty}/T_w)^p$ term is required in equation (12) so that corrected h_f/h_o results from the present study match measured results given in [1]. It is applied using

$$h_f/\bar{h}_o = h_f/h_o (T_w/T_{r\infty})^p \tag{13}$$

where $h_f/\bar{h}_o$ is determined from the $\theta = 0$ value extrapolated from measurements of $h/\bar{h}_o$ versus θ, or from measurements of $h/\bar{h}_o (T_{rc}/T_{r\infty})^n$ versus θ. Either way, the same $h_f/\bar{h}_o$ is obtained since $(T_{rc}/T_{r\infty})^n = 1$ at at $\theta = 0$. In equation form

$$h/\bar{h}_o (T_{rc}/T_{r\infty})^n = h_f/\bar{h}_o (1-\eta\theta) \tag{14}$$

Alternatively,

$$h^*/h_o = h_f/\bar{h}_o (1-\eta\theta) \tag{15}$$

where h^*/h_o is partially corrected "artificial" value of $h/\bar{h}_o$, defined for convenience. The value of p in (13) giving the best fit between present results and those from [1] is 0.40. Although valid over a range of injection rates, equation (13) is applied only for the one $(T_w/T_{r\infty})$ ratio of the present study.

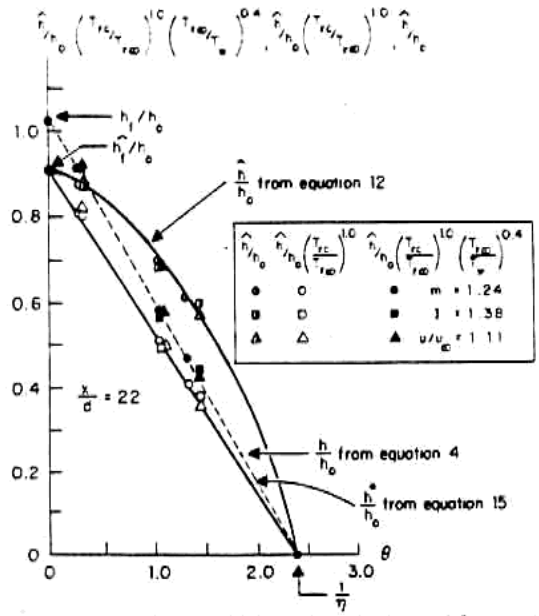

Fig. 8(a) h/h_o, $h/h_o(T_{rc}/T_{r\infty})^{1.0}$, and $h/h_o(T_{rc}/T_{r\infty})^{1.0}(T_{r\infty}/T_w)^{0.4}$ versus θ

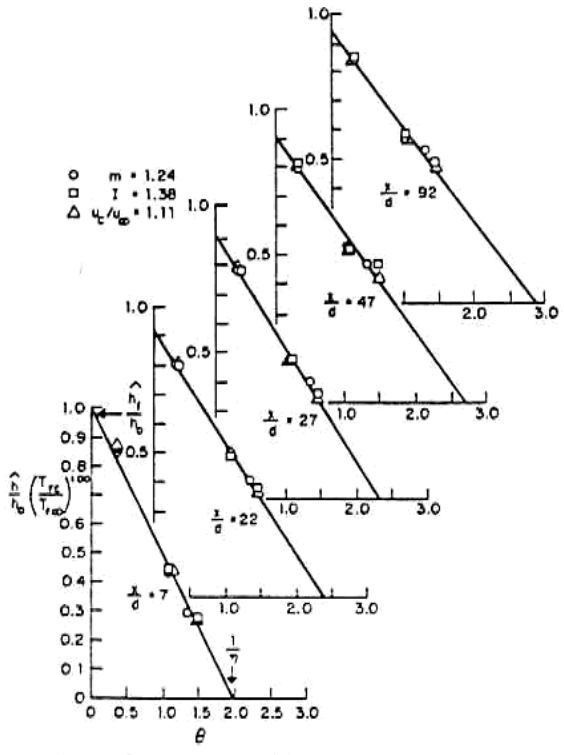

Fig. 8(b) $h/h_o(T_{rc}/T_{r\infty})^{1.0}$ versus θ for different x/d

In Fig. 8(a) are shown: (a) variable property h/h_o from equation (12), (b) h^*/h_o from equation (15), and (c) constant property h/h_o from equation (4). These lines correspond to h/h_o, $h/h_o(T_{rc}/T_{r\infty})^{1.0}$, and $h/h_o(T_{rc}/T_{r\infty})^{1.0}(T_{r\infty}/T_w)^{0.40}$ data, respectively, where the latter two show a linear variation with θ. The overall effect of variable properties is evident from h/h_o and h/h_o results in Fig. 8(a), and from the equation

$$h/h_o(T_{rc}/T_{r\infty})^n(T_{r\infty}/T_w)^r = h/h_o \qquad (16)$$

The correction term includes the effect of variable density ratio, ρ_c/ρ_∞. It is dependent on nondimensional coolant temperature θ and should be considered valid only over the nondimensional coolant temperature range of the present measurements: $0 \le \theta < 1.5$.

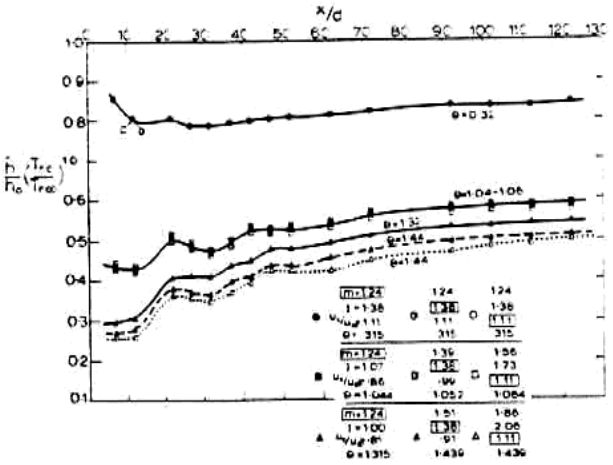

Fig. 9 Variation of $h/h_o(T_{rc}/T_{r\infty})^{1.0}$ with x/d

(d) Dependence of $h/h_o(T_{rc}/T_{r\infty})^n$ on θ and x/d. In order to show the effect of the portion of the correction term pertaining to adiabatic effectiveness, results in $h/h_o(T_{rc}/T_{r\infty})^{1.00}$ versus θ coordinates are given in Fig. 8(b) for five different values of x/d. These results were obtained for $m = 1.24$, $I = 1.38$, and $U_c/U_\infty = 1.11$. Referring to Fig. 4, lines corresponding to these three injection parameters intersect at run number 599. Such intersection points will be referred to as "match points," required in order to provide a suitable basis for comparison of results for the three parameters m, I, and U_c/U_∞. "Match points" were chosen on the experimental domain map of Fig. 4 at the minimum θ where measured data were obtained. The smallest θ was chosen for this purpose in order to obtain the largest differences in the abscissa intercepts of $h/h_o(T_{rc}/T_{r\infty})^n$ versus θ lines.

According to Fig. 8(b), variations of $h/h_o(T_{rc}/T_{r\infty})^{1.00}$ with θ obtained for $m = 1.24$, $I = 1.38$, and $U_c/U_\infty = 1.11$ lie along the same line regardless of which parameter is held constant. Such behavior results due to the dependence of h/h_o on injection parameters in the film-cooled thermal boundary layer, as evident from results presented in Fig. 5. Here h/h_o shows a very weak dependence on all injection parameters for $m > 1.4$. Thus the fact that data for constant I, and U_c/U_∞ are along the same line in 8 is not expected for all magnitudes of injection parameters.

The results shown in Fig. 8(b) are again given in Fig. 9 along with additional data. In this figure, $h/h_o(T_{rc}/T_{r\infty})^{1.0}$ is given as it varies with x/d for a variety of experimental conditions. The increase of normalized h with downstream distance is particularly evident for $\theta = 1.32$–1.44. As for Fig. 8, the results in Fig. 9 were determined at measurement points along lines of constant m, I, and U_c/U_∞ emanating from run number point 599 in Fig. 4. Thus three sets of data each are presented for hot, ambient, and cold injection, where all three data sets for hot injection ($\theta = .315$) are the same since they correspond to the same run number. Even though different data sets were used to determine results for $\theta = 1.04$–$.1.06$, the three curves in Fig. 9 are nearly the same. For $\theta = 1.32$–1.44, the $h/h_o(T_{rc}/T_{r\infty})^{1.0}$ data are slightly different at a given x/d, mostly from slightly different θ. Results such as those in Fig. 9 are useful, since they may be used with Fig. 8 type plots in order to determine the variation of the adiabatic film-cooling effectiveness with downstream distance.

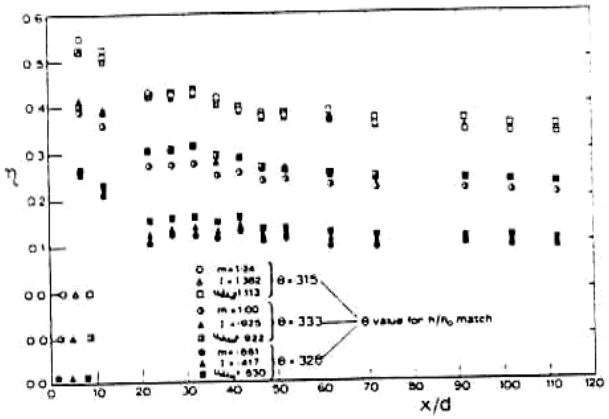

Fig. 10 Adiabatic film cooling effectiveness versus x/d as different injection parameters are held constant

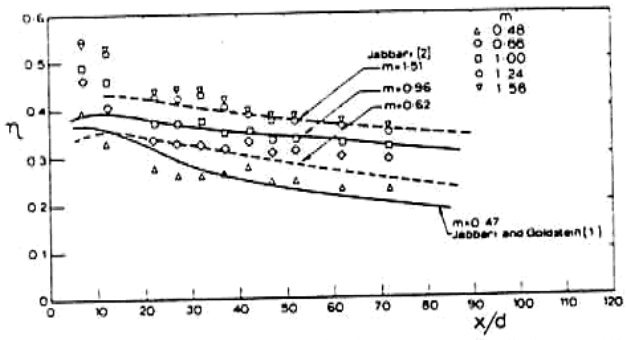

Fig. 11 Comparison of adiabatic film cooling effectiveness with results from [1] and [2]

(e) Adiabatic Film-Cooling Effectiveness. The adiabatic film-cooling effectiveness is presented in Fig. 10 at it varies with x/d. Results are shown deduced from the same family of data presented in Figs. 8 and 9, along with results from two additional families of data. Values of θ for the $h/\bar{h}_o$ "match point" are indicated on the figure, and always lie between 0.315 and 0.333. As one expects from results in Figs. 8 and 9, the magnitude of η at a given x/d is nearly the same regardless of whether $m = 1.24$, $I = 1.38$, or $U_c/U_\infty = 1.11$. For lower values of these injection parameters, small differences are evident between the m, I, and U_c/U_∞ results in a given family. Generally, results for constant U_c/U_∞ are several percent higher than the constant I results, which are slightly higher than results at constant m. Thus, from Fig. 10, the effect of using constant m, I, or U_c/U_∞ along a $h/\bar{h}_o(T_{rc}/T_{r\infty})^n$ versus θ line results in effectiveness differences which are no greater than ± 10 percent.

In Fig. 11, η results are presented which were deduced by using equation (12) with $n = 1.00$ for $m = .66$, 1.00, 1.24, and 1.56, and $n = 0.80$ for $m = .48$. At a given value of x/d, values of η increase with m, until $m > 1.24$, when further increases in the injection mass flux ratio do not provide higher film cooling effectiveness. At a given mass flux ratio, the effectiveness generally decreases with downstream distance. For $x/d > 20$, Fig. 11 shows that magnitudes of η for $m = 1.00$ and $m = 1.56$ agree with Jabbari's [2] measurements at approximately the same injection ratios with a maximum deviation of 10 percent. At $m = 0.66$ and $m = 0.48$ the maximum deviation is about 15 percent. Without the $T_{rc}/T_{r\infty}$ term in equation (12), estimated values of η have magnitudes which are one-third to one-half of constant property values at $m = 1.00$. Thus, for $x/d > 20$, the validity of equation (12) is supported by measurements obtained at injection mass flux ratios ranging from .48 to 1.56, indicating that the adiabatic film-cooling effectiveness for constant property flow can be deduced from heat transfer measured in a compressible, variable property environment.

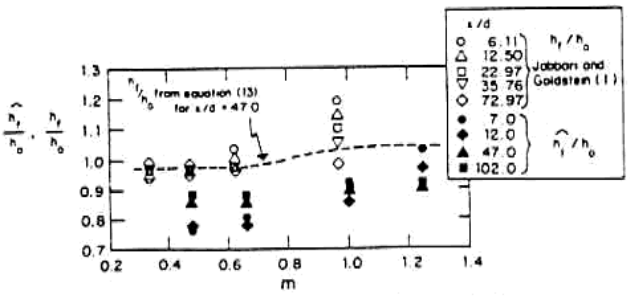

Fig. 12 Normalized film cooling heat transfer coefficients based on the $(T_{AW} - T_W)$ temperature difference

The differences between the present results and those from [1] and [2] for $x/d < 20$ are believed to be due to three-dimensional flow near injection holes. According to these sources, h_f' and η' are nonuniform in the spanwise direction for $x/d < 20$ with periodic variations dependent on the minimum spanwise distance between injection holes. The local effectiveness η' is not equal to the spanwise average effectiveness η, and equation (5) is not valid. For $x/d > 20$, η' and h_f' become invariant in the cross-stream direction, and equation (5) is valid allowing determination of η from variable property heat transfer measurements.

(f) Heat Transfer Coefficients Based on the $(T_{AW} - T_W)$ Temperature Difference. The variation of $h_f/\bar{h}_o$ with m is shown in Fig. 12, along with h_f/h_o results from [1]. Magnitudes of $h_f/\bar{h}_o$ were determined from ordinate intercepts of $h/\bar{h}_o$ $(T_{rc}/T_{r\infty})^n$ versus θ lines, as indicated in Fig. 8. Using this procedure, $h_f/\bar{h}_o$ are not dependent on the $(T_{rc}/T_{r\infty})^n$ term in equation (12), because this ratio has the value unity at $\theta = 0$.

The $h_f/\bar{h}_o$ results from the present study are 10–20 percent lower than constant property results from [1]. However, at a given x/d, the trends with m from the two sources are similar. At the largest x/d for the two studies (102.0 and 72.97 for [1]), normalized coefficients are nearly constant as m varies. At $x/d \equiv 6$–7, $h_f/\bar{h}_o$ and h_f/h_o variations with m are larger than results at all other x/d.

Using $p = 0.40$ in equation (13), values of h_f/h_o were calculated from $h_f/\bar{h}_o$ data at $x/d = 47.0$. These corrected h_f/h_o are represented by the dashed line in Fig. 12 and provide a good match with constant property data at about the same x/d. Equally good agreement between corrected h_f/h_o and measured values from [1] is also found for other $x/d > 20$.

5 Conclusions

An empirical variable property correction for film-cooled turbulent boundary layers is presented. This correction was determined from measurements in a turbulent boundary layer at $M_\infty = 0.64$, $P_{0\infty} = 2.9 \times 10^5$ N/m^2, $T_w \equiv 290$ K and $T_{r\infty} \equiv 403$ K which was film-cooled using two staggered rows of injection holes inclined at 35 deg. The temperature ratio product $(T_{rc}/T_{r\infty})^n(T_{r\infty}/T_w)^p$ is used for the correction as included in the equation

$$h/\bar{h}_o(T_{rc}/T_{r\infty})^n(T_{r\infty}/T_w)^p = h_f/h_o(1 - \eta\theta) \qquad (12)$$

$n = 1.0$ gives the best fit between η values from the present study and those from the University of Minnesota [1, 2] for $.65 < m < 1.6$ and $n = 0.8$ gives the best fit for $m = 0.48$. $p = 0.40$ gives the best fit of h_f/h_o results from the present study to those from [1] for $0.48 < m < 1.00$ and $x/d > 20$.

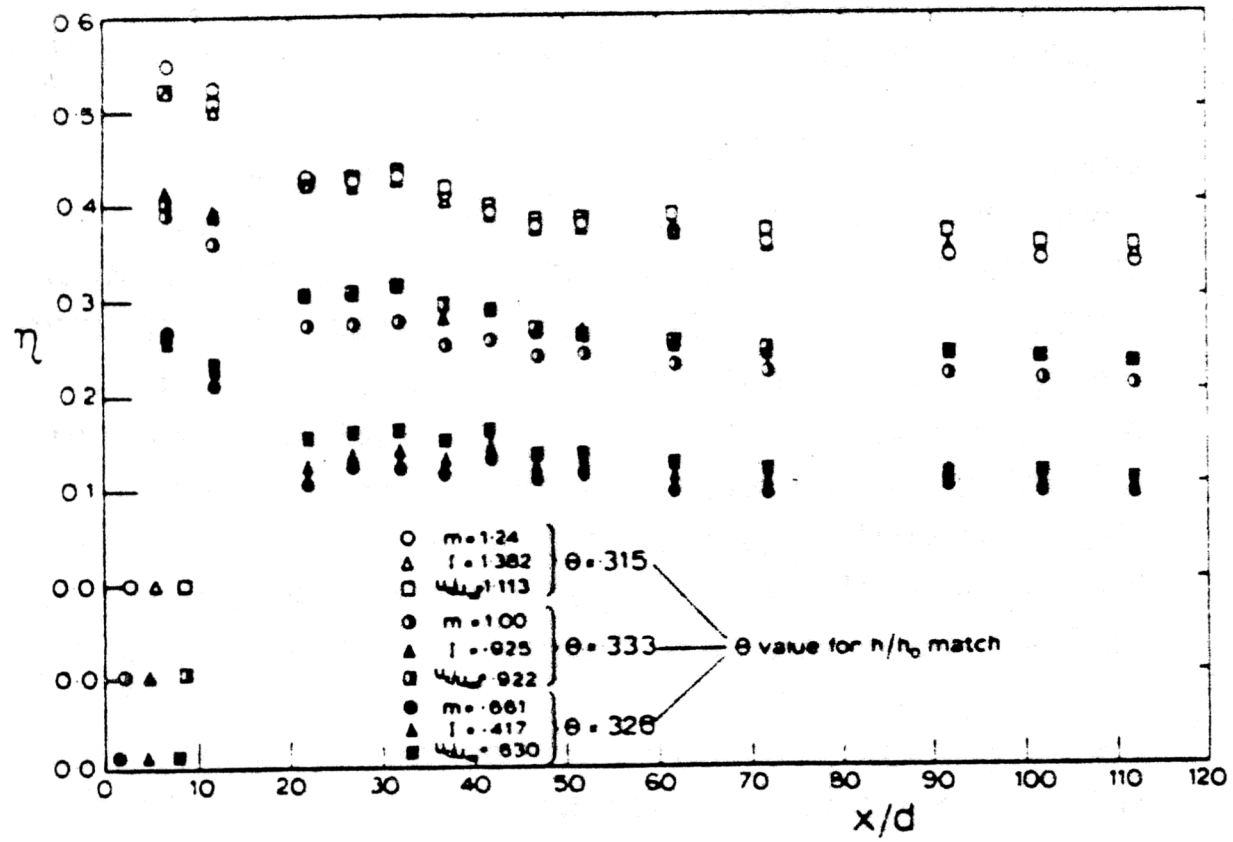

Fig. 10 Adiabatic film cooling effectiveness versus *x/d* as different injection parameters are held constant

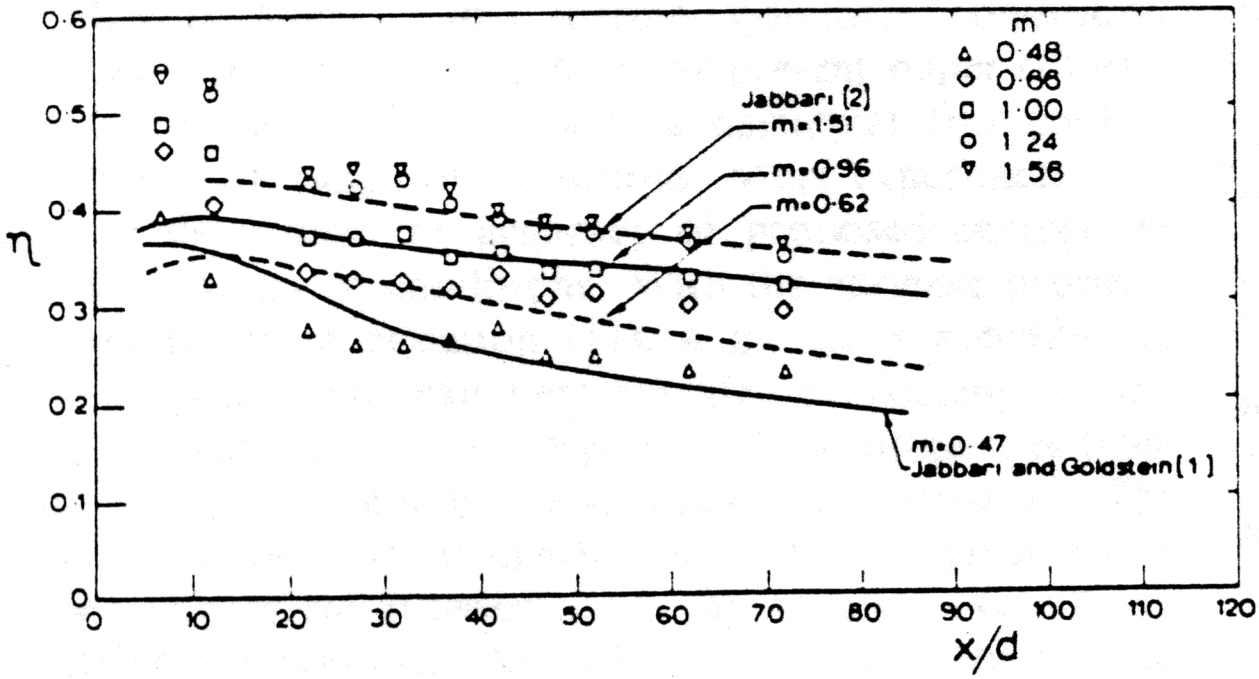

Fig. 11 Comparison of adiabatic film cooling effectiveness with results from [1] and [2]

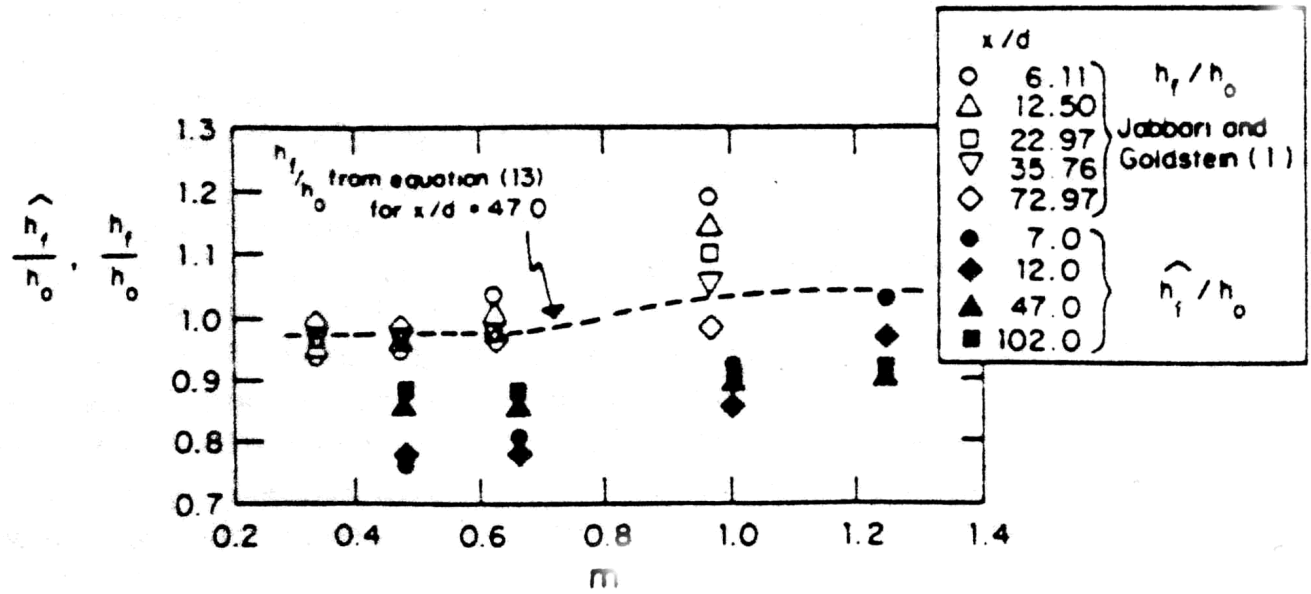

Fig. 12 Normalized film cooling heat transfer coefficients based on the $(T_{AW} - T_W)$ temperature difference

Equation (12) is useful for $\theta < 1.5$, where it provides a means to determine changes of $h/\hat{h}_o$ due to variable properties (including varying density ratio) in film-cooled turbulent boundary layers. All terms on the right-hand side of (12) are for constant properties, whereas $h/\hat{h}_o$ is a variable property term.

In order to deduce constant property η from variable property $h/\hat{h}_o$, plots of $h/\hat{h}_o(T_{rc}/T_{r\infty})^n$ versus θ were used. Because m, I, and U_c/U_∞ all vary with θ in the compressible environment, the question arises as to which injection parameter to keep constant in the heat transfer plots. Measurements indicate that the η in best agreement with constant property measurements is obtained when the injection mass flux ratio m is held constant. However, differences in η obtained as m, I or U_c/U_∞ are held constant and are never greater than $\pm$ 10 percent, and nearly zero for $1.24 \leq m \leq 1.56$.

Variable property, film-cooled turbulent boundary layers are complex thermal-fluid systems. A complete variable property correction would depend on injection system geometry, injection flow rate parameters, all important temperatures, the fluid mechanics of the flow, the fluid mechanics of the injection jets, the type of fluid, compressibility parameters, and thermal boundary conditions. The variable property equation of the present paper offers a simple correction for a flow with a particular film-cooling geometry over a range of conditions. More experiments are needed to determine the accuracy of proposed corrections over wider ranges of conditions. With the variable property correction terms in equation (12), a means is provided to determine isothermal wall heat transfer coefficients in environments with temperature dependent fluid properties from constant property h_f and η data available in the literature. The equation also allows determination of $h/\hat{h}_o$ at a given θ in a variable property environment, provided data are available at two other θ less than 1.5. As such, the results of the present paper give an indication of the importance of variable properties in film-cooled turbulent boundary layers, and hopefully, will provoke more attention and discussion to this area.

Acknowledgments

Mr. Rogier Conniasselle is the technical engineer for the von Karman Institute CT-2 facility used for the present study. The authors also acknowledge the helpful comments of three anonymous referees. Mr. M. Pezzani, Professor R. J. Goldstein, and Professor R. J. Moffat are to be thanked for fruitful discussions on the research. Professor P. Bradshaw provided several useful comments after reading the first draft of the manuscript. The support of Professor J. J. Ginoux, Director of the von Karman Institute, is also much appreciated by the authors.

References

1 Jabbari, M. Y., and Goldstein, R. J., "Adiabatic Wall Temperature and Heat Transfer Downstream of Injection Through Two Rows of Holes," ASME *Journal of Engineering for Power*, Vol. 100, April 1978, pp. 303–307.

2 Jabbari, M. Y., "Film Cooling and Heat Transfer with Air Injection Through a Staggered Row of Holes into an Accelerating Flow," Ph.D. Thesis, University of Minnesota, Minneapolis, Minn., 1973.

3 Pedersen, D. R., Eckert, E. R. G., and Goldstein, R. J., "Film Cooling with Large Density Differences Between the Mainstream and the Secondary Fluid Measured by the Heat Mass Transfer Analogy," ASME JOURNAL OF HEAT TRANSFER, Vol. 99, Nov. 1977, pp. 620–627.

4 Goldstein, R. J., Eckert, E. R. G., and Burggraf, F., "Effects of Hole Geometry and Density on Three-Dimensional Film Cooling," *International Journal of Heat and Mass Transfer*, Vol. 17, 1973, pp. 595–607.

5 Foster N. W., and Lampard, D., "Effects of Density and Velocity Ratio on Discrete Hole Film Cooling," *AIAA Journal*, Vol. 13, No. 8, Aug. 1975, pp. 1112–1114.

6 Choe, H., Kays, W. M., and Moffat, R. J., "The Turbulent Boundary Layer on a Full Coverage Film Cooled Surface. An Experimental Heat Transfer Study with Normal Injection," Report HMT-11, Stanford University, May 1975.

7 Moffat, R. J., "Full-Coverage Film Cooling," Film Cooling and Turbine Blade Heat Transfer, VKI LS 1982-03, von Karman Institute for Fluid Dynamics, Rhode-St-Genese, Feb. 22–26, 1982.

8 Metzger, D. E., Carper, H. J., and Swank, L. R., "Heat Transfer with Film Cooling Near Nontangential Injection Slots," *Journal of Engineering for Power*, Apr. 1968, pp. 157–163.

9 Metzger, D. E., and Fletcher, D. D., "Evaluation of Heat Transfer for Film-Cooled Components," *Journal of Aircraft*, Vol. 8, No. 1, Jan. 1971, pp. 33–38.

10 Eckert, E. R. G., Goldstein, R. J., and Pedersen, D. R., "Comment on 'Evaluation of Heat Transfer for Film-Cooled Turbine Components,'" *Journal of Aircraft*, Vol. 18, No. 1, Jan. 1971, pp. 63–64.

11 Eckert, E. R. G., "Analysis of Film Cooling and Full-Coverage Film Cooling of Gas Turbine Blades," Tokyo International Gas Turbine Congress, 83-TOKYO-IGTC-15, ASME-83-GTJ-2, 1983.

12 Paradis, M. A., "Film Cooling of Gas Turbine Blades: a Study of the Effect of Large Temperature Differences on Film Cooling Effectiveness," ASME *Journal of Engineering for Power*, Vol. 99, No. 1, Jan. 1977, pp. 1–10.

13 Ligrani, P. M., and Breugelmans, F. A. E., "Turbine Blade Cooling Research at the von Karman Institute for Fluid Dynamics," Fifth International Symposium on Air Breathing Engines, Bangalore, India, Feb. 16–21, 1981.

14 Consigny, H., and Richards, B. E., "Short Duration Measurements of Heat Transfer Rate to a Gas Turbine Rotor Blade," ASME *Journal of Engineering for Power*, Vol. 104, No. 3, July, 1982, pp. 542–551.

15 Schultz, D. L., Jones, T. V., Oldfield, M. L. G., and Daniels, L. C., "A New Transient Facility for the Measurement of Heat Transfer Rates," *AGARD Conference Proceedings No. 229, High Temperature Problems in Gas Turbine Engines*, Sept. 1977, pp. 33-1–31–27.

16 Schlichting, H., *Boundary Layer Theory* (6th ed.), McGraw-Hill, New York, 1968.

17 Kays, W. M., and Crawford, M .E., *Convective Heat and Mass Transfer* (2d ed.), McGraw-Hill, New York, 1980.

18 Ligrani, P. M., Camci, C., and Grady, M. S., "Thin Film Heat Transfer Gage Construction and Measurement Details," VKI Technical Memorandum 33, von Karman Institute for Fluid Dynamics, Rhode-St-Genese, Nov. 1982.

19 Oldfield, M. L. G., Jones, T. V., and Schultz, D. L., "On-Line Computer for Transient Turbine Casade Instrumentation," *IEEE Transactions on Aerospace and Electronics Systems*, Vol. AES-14, No. 5, Sept. 1978, pp. 738–749.

20 Benmansour, S., "Discharge Coefficients of Film Cooling Holes," M. Phil. thesis, University of Nottingham, Nottingham, 1981.

21 Papell, S. S., and Trout, A. M., "Experimental Investigation of Air Film Cooling Applied to an Adiabatic Wall by Means of an Axially Discharging Slot," NASA TN D-9, 1959.